Intrinsic origin of interface states and band-offset profiling of nanostructured $LaAlO_3/SrTiO_3$ heterojunctions probed by element-specific resonant spectroscopies

G. Drera,[1] G. Salvinelli,[1] F. Bondino,[2] E. Magnano,[2] M. Huijben,[3] A. Brinkman,[3] and L. Sangaletti[1]

[1]*I-LAMP and Dipartimento di Matematica e Fisica, Università Cattolica, Via dei Musei 41, 25121 Brescia, Italy*

[2]*IOM-CNR, TASC Laboratory, S.S.14 Km 163,5 Basovizza, 34149 Trieste, Italy*

[3]*Faculty of Science and Technology and MESA+ Institute for Nanotechnology, University of Twente, 7500 AE Enschede, The Netherlands*

(Received 13 March 2014; revised manuscript received 5 June 2014; published 17 July 2014)

The origin of electronic states at the basis of the 2DEG found in conducting $LaAlO_3/SrTiO_3$ interfaces (5 u.c. $LaAlO_3$) is investigated by resonant photoemission experiments at the Ti $L_{2,3}$ and La $M_{4,5}$ edges. As shown by the resonant enhancement at the Ti $L_{2,3}$ edge, electronic states at E_F receive a dominant contribution from Ti $3d$ states. Both Ti and La resonance effects in the valence-band region are used to estimate the valence-band maxima at the two sides of the junction. Through a comparison with the valence-band states of the $LaAlO_3$ and $SrTiO_3$ parent compounds, we reconstruct the band diagram of the heterojunction, which is revealed to be type I (straddling gap), with a large notch of the band profile at the interface as compared with the reference insulating (3 u.c. $LaAlO_3$) interface.

DOI: 10.1103/PhysRevB.90.035124 PACS number(s): 73.21.−b, 78.70.Dm, 79.60.−i, 77.65.−j

I. INTRODUCTION

Interfaces between perovskite oxides can display properties at the nanometer scale that are qualitatively different from their single building blocks, allowing one to engineer novel functionalities through the growth of epitaxial heterostructures. Indeed, the discovery of a two-dimensional electron gas (2DEG) at the interface between two perovskite oxides, i.e., lanthanum aluminate ($LaAlO_3$, LAO) and strontium titanate ($SrTiO_3$, STO) [1,2], has disclosed unexpected perspectives in the physics of oxide-based junctions. So far, a large number of studies have attempted to determine the physical properties of the 2DEG and to develop novel devices based on the capability to control the interface properties through chemical interactions at the surface, suitable materials combination, or strain engineering [3].

In this scenario, the study of the electronic properties of $LaAlO_3/SrTiO_3$ (LAO/STO) heterojunctions (HJs) can provide fundamental information to understand the origin of the relevant physical phenomena observed in these systems, namely, magnetism, superconductivity, and the buildup of 2DEG at the interface [2,4–8]. On the other hand, a profiling of energy-level alignment across the heterointerface would disclose the basic information for the design, characterization, and tuning of devices based on the intrinsic electric fields arising at the interface. Photovoltaics [9,10], field-effect transistors [11], and devices based on tunable conductivity and charge writing [12,13] are among the applications that would benefit from detailed characterization of band profiling across the HJ. However, only one study based on cross-sectional scanning tunneling microscopy [14] has reported a direct evidence of the potential profile in a LAO-STO heterojunction, grown at 850 °C in a 2×10^{-5} mbar $P(O_2)$.

The electronic properties are mainly determined by electronic states close to, or at, the Fermi level (E_F) in the conducting LAO-STO heterojunctions. These states have been observed by ultra-violet photoemission spectroscopy by Siemons *et al.* [15], but further investigations were basically hindered by the low intensity of the photoemission process from a buried interface. For this reason, these states have been searched for by resonant photoemission spectroscopy (ResPES) and have been evidenced by Drera *et al.*[16] in both insulating and conducting samples. As the resonant enhancement was observed at the Ti $2p$-$3d$ absorption threshold, the element-specific ResPES technique indicates that the in-gap states have a Ti character and are ascribed to a $3d^1$ configuration of a formally Ti^{3+} ion. Soon after, these states were also evidenced by Koitzsch *et al.* [17] in an attempt to relate their line shape and energy to the oxygen stoichiometry. Recently, Cancellieri *et al.* [18], at odds with Refs. [16] and [17], have shown that the $3d^1$ states are absent in insulating systems, while they are clearly detected by ResPES in conducting samples. Finally, in a recent k-resolved ResPES experiment, two distinct features (one in-gap and the other at E_F) have been singled out in a conducting LAO-STO HJ [19]. All these results are still providing a rather scattered scenario (see also Ref. [20] for further discussions), which is strongly dependent on details of the STO surface preparation, sample growth, and postgrowth treatment, in spite of common features (namely, Ti-O termination of the STO substrate and number of LAO unit cells grown above the substrate) that would render the samples nominally identical. Contrasting results also appeared on band alignment profiling based on x-ray photoemission spectra [21–23], resulting in different junctions (type I or type II) and LAO band gradients.

In this study, we address the problem of the origin of electronic states at the Fermi level of a 5-unit-cell (u.c.) conducting LAO-STO sample on the basis of element-specific resonant electronic spectroscopies. It is shown that these spectroscopies can provide an unambiguous characterization of the chemical bonds contributing to the density of states in the Fermi level region and can be used to track a profile of the electronic levels across the heterojunction.

The spectral weight of both Ti $3d$ and La $4f$ states in the valence-band region is probed. This allowed us (i) to determine the energy of the valence-band maximum on both sides of the junction that will be used to track the band bending, and (ii) to probe that the interface states (IS) at the Fermi level have a dominant Ti $3d$ character. The origin of the spectral weight at E_F is discussed also by referring to the effect of oxygen

vacancies and to intermixing and cation substitution effects that may occur at the interface [24–26].

Furthermore, the band alignment profiling shows similarities between the conducting and the insulating samples, both of which were shown to be type I (straddling gap), though the conducting sample presents deeper notches in the energy levels at the interface.

Unlike previous studies based on hard x-ray photoemission [22], that are more sensitive to the bulk of the samples and therefore can probe the electronic properties well below the interface, the present results, obtained with soft x rays, allowed us to unambiguously probe the extent of band bending at the interface, filling the gap in the experimental tracking of band offsets in the LAO-STO system.

II. EXPERIMENTAL AND COMPUTATIONAL DETAILS

The LAO-STO heterostructures (HSs) have been grown by pulsed laser deposition (PLD) at the MESA$^+$ Institute for Nanotechnology, University of Twente. A conducting 5-u.c. sample and an insulating 3-u.c. sample have been grown on TiO_2-terminated $SrTiO_3$ single crystal. We shall focus on the 5-u.c. sample, while the 3-u.c. sample is used as a reference to discuss the specific properties related to the 2DEG in the conducting sample. The two n-type 3-u.c. and 5-u.c. LAO-STO samples were grown at $P_{O_2} \sim 10^{-3}$ mbar oxygen partial pressure. The 3-u.c. sample showed a sheet resistance above 1GΩ/sq, while the conducting 5-u.c. sample showed a sheet resistance of 5.5 kΩ/sq at 300 K. According the the systematic study reported in Ref. [7], the P_{O_2} during the growth should rule out the presence of oxygen vacancies in both HJs. In Ref. [20] the present samples have been thoroughly characterized by core-level photoemission and transport measurements.

Photoemission and x-ray absorption experiments have been carried out at the BACH beamline of the Elettra synchrotron light source in Trieste (Italy). All data have been collected at room temperature with a Scienta R3000 electron spectrometer. The samples have been grounded by contacting the pads used for transport measurements. Resonant photoemission spectra of the 5-u.c. sample have been aligned to a reference gold clip in contact with the sample. The insulating 3-u.c. sample showed a slow charging effect, as compared to the time required for a scan, upon measurement. To obtain a good signal-to-noise ratio, we collected single fast scans of the valence-band region and then we summed up these spectra after alignment to the maximum of the Ti^{4+} resonance at a binding energy BE = 7.5 eV. This spectrum was then aligned to the 5-u.c. sample by referring to the centroid of the resonant emission of Ti^{4+} states in the 6.5–9.5 eV BE range.

STO and LAO projected density of states have been calculated with density functional theory in the local density approximation (LDA) for the bulk single crystals; computations have been carried out with the ABINIT code [27] with the projector augmented-wave (PAW) method. These calculations are aimed at identifying the spectral weight distribution of bulk LAO or STO electronic states in the valence-band region, to be used as a reference to proceed with the experimental analysis of energy shifts.

Evaluation of the photoemission signal attenuation due to the LAO layer was carried out by Monte Carlo calculations of the depth distribution function (DDF). The photoemission peak intensity of a selected layer at a depth d with a thickness t has been evaluated with the following formula:

$$I(E_k,\theta,\psi,\sigma,\beta) = K(\sigma)\int_d^{d+t} \Phi(E_k,\theta,\psi,\beta,z)dz, \quad (1)$$

where K is a constant which includes the total photoionization cross section σ [28], the atomic density of the species, and the analyzer response parameters; θ (ψ) is the angle between the sample normal and the analyzer (source), E_k is the electron kinetic energy and β the photoionization asymmetry parameter; and $\Phi(z)$ is the DDF, which describes the probability of an electron photoemitted at depth z to reach the analyzer. The DDF has been evaluated in the transport approximation (TA) with the Monte Carlo algorithm described by Werner [29]; in the TA approach both the inelastic and isotropic-elastic mean free path, obtained by TPP-2M formula [30] and in Ref. [31], are properly considered in each oxide layer.

III. RESULTS AND DISCUSSION

A. Character of interface states

Resonant photoemission spectroscopy experiments carried out by scanning the photon energy at the Ti $L_{2,3}$ edge provide the opportunity to emphasize titanium-related electronic states in the valence-band region up to E_F that would be otherwise missed by an off-resonance tuning of the photon energy. In a ResPES experiment, the valence-band photoemission spectra are collected by changing the photon energy across an absorption edge. In this condition, for a $3d$ transition metal, the direct photoemission channel ($3d^n \rightarrow 3d^{n-1} + e^-$) can interfere with the autoionization channel triggered by the creation of a core hole ($2p^5 3d^{n+1} \rightarrow 2p^6 3d^{n-1} + e^-$). A schematic view of the process is depicted in Fig. 1 (left panel). Channel 1 is the direct photoemission process, whereas channel 2a is the $2p$-$3d$ photon absorption, which is followed by the autoionization process (channel 2b). When the photon energy is increased above the absorption threshold, the autoionization process ultimately turns into the normal Auger emission and the interference effects are lost. This transition is denoted as resonant Raman Auger (RRAS) to normal Auger emission [32] and is related to the dynamics of the electrons excited into the empty states upon photon absorption. The RRAS emission is an N-1 electron final state that occurs at constant BE, while the normal Auger emission is an N-2 electron final state found at constant kinetic energy. Therefore, if all spectra are aligned on the BE scale, the constant BE resonating features are those ascribed to RRAS, while those apparently dispersing on the BE scale are the normal Auger features.

In a configuration interaction (CI) approach, the ground state (g.s.) of a Ti ion is described as (see, e.g., Ref. [33])

$$\Psi_{g.s.} = \alpha_0|3d^n\rangle + \alpha_1|3d^{n+1}\underline{L}^1\rangle + \alpha_2|3d^{n+2}\underline{L}^2\rangle \quad (2)$$

(where $n = 0$ and $n = 1$ for Ti^{4+} and Ti^{3+} ions, respectively), while the final state of the x-ray absorption spectroscopy

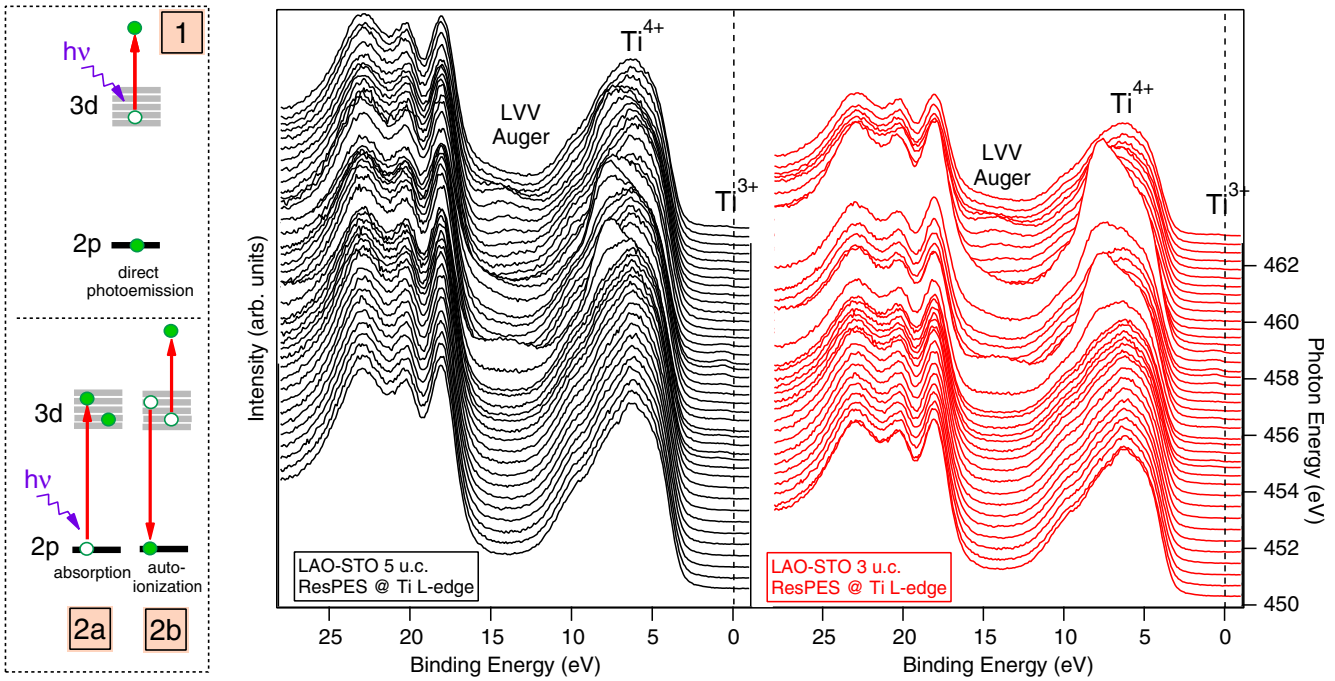

FIG. 1. (Color online) Sketch of the two excitation channels (1, $2a + 2b$) that can quantum mechanically interfere in a ResPES process (left panel). Resonant photoemission data at the Ti $L_{2,3}$ edge of the 5-u.c. (mid panel) and 3-u.c. (right panel) LAO-STO samples, normalized to the incident photon intensity.

(XAS) process (i.e., the intermediate state of the autoionization channel, i.s.) is

$$\Psi_{\text{i.s.}} = \beta_0|\underline{2p}3d^{n+1}\rangle + \beta_1|\underline{2p}3d^{n+2}\underline{L}^1\rangle + \beta_2|\underline{2p}3d^{n+3}\underline{L}^2\rangle, \tag{3}$$

and finally the photoemission channel (finale state, f.s.) is

$$\Psi_{\text{f.s.}} = \gamma_0|3d^{n-1}\rangle + \gamma_1|3d^n\underline{L}^1\rangle + \gamma_2|3d^{n+1}\underline{L}^2\rangle, \tag{4}$$

which can be reached either directly from the ground state or through autoionization from the intermediate state. The $|3d^{n-1}\underline{L}^1\rangle$ configuration is absent in the case of the Ti^{4+} ion. Here $\underline{L}$ and $\underline{2p}$ stand for an O $2p$ and a Ti $2p$ hole, respectively. The $|3d^n\underline{L}^{\overline{m}}\rangle$-like configurations are those accounting for charge transfer (CT) effects from the anion $2p$ to the transition metal (TM) $3d$ orbitals, providing a straightforward tool to consider the effect of Ti $3d$-O $2p$ bonding in CI calculations. The possibility to observe ResPES effects in the formally empty $3d$ shell of the Ti^{4+} cation is due to the presence of CT-like configurations, both in the initial and final states, whereas ResPES effects can also involve the ionic $|3d^1\rangle$ configuration in a Ti^{3+} cation.

The ResPES spectra collected at the Ti $L_{2,3}$ absorption edge of the 3-u.c. and 5-u.c. LAO-STO samples are shown in Fig. 1, right and mid panels, respectively. For both samples, the overall photoemission intensity in the valence-band (VB) region follows the shape of the XAS spectrum, as is shown in detail in Fig. 2 for selected peaks. In particular, in the 5–10 eV BE energy range, resonating features related to bulk STO Ti^{4+} energy levels can be detected. A careful inspection of the 0.0–1.5 eV BE range reveals the presence of additional electronic states (labeled as Ti^{3+} and hereafter denoted as interface states) that can be detected with photons at the Ti $L_{2,3}$ resonance conditions only.

Selected ResPES spectra collected from the 3-u.c. and 5-u.c. samples are shown in Fig. 2. The maximum intensity of the interface states [peak F in Figs. 2(a) and 2(b)] is obtained for a photon energy ($h\nu = 459.6$ eV) different from the energy where the maximum resonance of the main VB Ti^{4+} peaks (peaks D and E, maximum at $h\nu = 458.2$ eV) are detected.

Shallow core levels (A_1, A_2, A_3) do not display resonant enhancement at the Ti L edge, as they are related to photoemission from O $2p$, Sr $4p$, and La $4p$ core levels. Peak B is the Ti LVV Auger emission, while the shoulder C can be ascribed to the VB electronic structure distinctive of $LaAlO_3$, which in fact is more evident in the 5-u.c. sample. Consistent with a previous study on similar samples [16], interface states [Fig. 2(b)] are detectable also in the 3-u.c. sample, in the same energy region. The on-off resonance difference spectra [Fig. 2(a), gray area and dotted red line, hereafter denoted as resonant spectral weight, RSW] provides a direct probe of Ti $3d$ states of the uppermost STO layers and displays a maximum intensity at BE = 7.5 eV in both samples [peak G in Fig. 2(a)], while a shift of 0.3 eV can be detected between the VB edges [VBM_{3uc} and VBM_{5uc} in Fig. 2(a)], as well as in the La shallow core levels (A_2 and A_3) of the resonant spectra.

The unambiguous proof that Ti^{3+} ($3d^1$) states contribute to the spectral weight in the region below E_F is provided by the constant initial state (CIS) spectra [Fig. 2(c)], which follow the Ti $L_{2,3}$ XAS (due to bulk Ti^{4+} STO) in the main VB resonances [open squares in Fig. 2(c), whereas for the interface states the CIS data (filled circles) closely resemble the XAS profile of $LaTiO_3$ (a bulk Ti^{3+} compound [34])].

As a last comment on Fig. 2(b), it is worth observing that peak F resonates when the photon energy is tuned not only at one of the Ti^{3+} XAS peaks ($h\nu = 459.6$ eV), but also at the Ti^{4+} XAS peak ($h\nu = 458.2$ eV), although to a lower

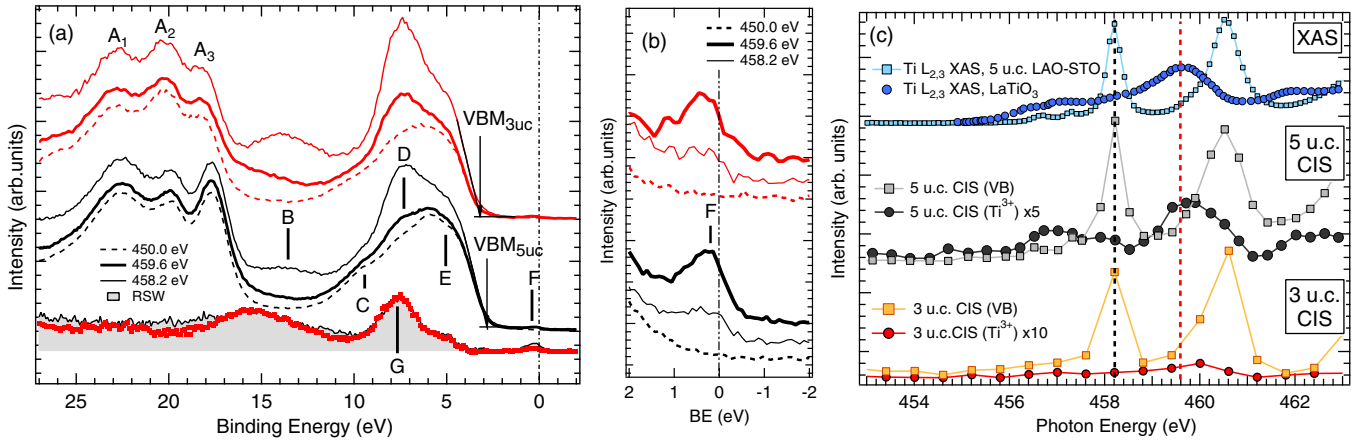

FIG. 2. (Color online) (A) Resonant photoemission spectra of insulating 3-u.c. (upper curves, red lines) and conductive 5-u.c. (lower curves, black lines) LAO-STO films, measured off-resonance (dashed line, $h\nu = 450$ eV), at Ti^{4+} resonance maximum (thin line, $h\nu = 458.2$ eV), and at the Ti^{3+} resonance maximum (thick line, $h\nu = 459.6$ eV). The vertical arrows mark the position of valence-band maxima (VBM-3 and VBM-5). Normalized RSW (off-resonance: $h\nu = 450$ eV; Ti^{3+} resonance: $h\nu = 459.6$ eV) of the 5 u.c. sample (shaded gray area) and of the 3-u.c. sample (dotted line). (B) Detailed view of the interface states F. Labels as in panel (A). For the two samples, the intensities have been normalized to the maxima of the peaks measured at $h\nu = 459.6$ eV. (C) CIS spectra on Ti^{3+} (filled circles, BE $= 1.0 \pm 1.0$ eV) and Ti^{4+} features (filled squares, BE $= 7.5 \pm 1.0$ eV); XAS spectra of the 5-u.c. sample (squares) and of a reference $LaTiO_3$ sample (circles). The vertical dashed lines mark the photon energies (458.2 and 459.6 eV) of the resonant spectra shown in panels (A) and (B).

extent. This can be explained by the fact that at 458.2 eV the intensity of the Ti^{3+} XAS profile [Fig. 2(c)] is not quenched and therefore also at this photon energy a weak Ti^{3+} resonance can be expected.

The CIS profile is collected by measuring the intensity profile of a selected photoemission peak (i.e., with constant binding energy) as the photon energy is scanned through the absorption threshold. In the simple case of a discrete level interfering with a continuum of states, the CIS line shape can be fit to a Fano profile $I(\epsilon)$ [35] according to the equation

$$I(\epsilon) \simeq \frac{(q+\epsilon)^2}{(\epsilon^2+1)}, \tag{5}$$

where

$$q = \frac{\langle \Psi_{3d}|\hat{\mathbf{r}}|\Psi_{2p}\rangle}{\pi V_{CK}\langle \Psi_{e_k}|\hat{\mathbf{r}}|\Psi_{3d}\rangle}, \tag{6}$$

with Ψ_{3d} representing the $3d$ TM states in the valence band, and $\epsilon = (h\nu - h\nu_0)/\Gamma$ is the reduced energy parameter and $\Gamma = 2\pi V_{CK}^2$, V_{CK} being the matrix element of the Coster-Kronig transition occurring in the autoionization process. Usually, when the CIS is measured at the TM $2p$-$3d$ absorption threshold, the $\langle \Psi_{3d}|\hat{\mathbf{r}}|\Psi_{2p}\rangle$ matrix element is quite large and the resulting CIS profile is very close to the absorption profile [36,37].

Although the photoemission spectra of the Ti^{3+} structures seem to be similar in insulating and conductive LAO-STO, their intensities are quite different, as shown by the different scaling factor of the CIS spectra in Fig. 2(c). By normalizing the RSW spectra at the 7.5-eV peak (Fig. 3, left panel), the relative ratio of 5-u.c. over 3-u.c. interface states becomes 5:1, in good agreement with the value (0.056:0.012) extracted from the Ti $2p$ core line analysis on the same compounds (see Table I in Ref. [20]).

The formation of photoinduced charge carriers either by x-ray or ambient light irradiation could be considered at the origin of the observed IS in the 3-u.c. sample, where they are not expected as the sample is insulating. As for soft x rays, we did not observe changes in the IS intensity upon

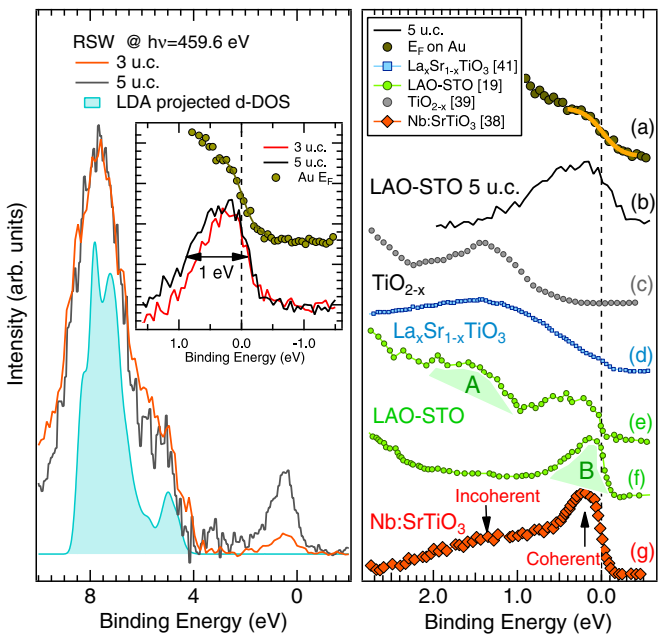

FIG. 3. (Color online) (Left) RSW spectra ($h\nu = 459.6$–450 eV) for the 3-u.c. and 5-u.c. LAO-STO samples, compared to DFT + U ($U = 8$ eV) d-projected DOS calculations of a STO bulk crystal. (Inset) High-resolution interface states spectra of the 5-u.c. and 3-u.c. HJs. The intensities have been normalized to the peak maxima. (Right) High-resolution spectra of the 5-u.c. sample interface states (b), Fermi edge of the gold film deposited on the clip in contact with the HJ (a), resonant spectra of the Nb:$SrTiO_3$ (adapted from Ref. [38]) (g), 5-u.c. LAO-STO (adapted from Ref. [19]) (e, f), $La_xSr_{1-x}TiO_3$ (adapted from Ref. [41]) (d), and TiO_{2-x} [39] (c).

exposure to synchrotron radiation for several days, ruling out the x-ray irradiation as a mechanism, unless the effect occurs immediately upon irradiation and remains constant over several days. The sensitivity of LAO-STO samples to ambient light is well known, to such an extent that transport measurements are carried out on samples stored in the dark for a long time. In any case, as these effects should occur on the STO side of the junction to yield Ti^{3+} electronic states, it is still difficult to justify the lower intensity observed for the 3-u.c. sample with respect to the 5-u.c. sample. In fact, irradiation effects are supposed to be larger in the 3-u.c. than in the 5-u.c. sample, due to the thinner LAO overlayer on top of the STO substrate, suggesting that the 5-u.c. sample displays an extra intensity with a different origin that adds up to the weak spectral weight observed in the 3-u.c. sample. To proceed with our study, at the present stage we regard the IS observed in the 3-u.c. sample as due to an extrinsic effect, while the higher intensity of the resonant IS emission for the 5-u.c. sample is considered as a signature of an extra emission related to the presence of the 2DEG.

High-resolution spectra (inset of Fig. 3, left panel) on the Ti^{3+} peaks reveal an asymmetric line shape. Both in the insulating and in the conducting LAO-STO samples, these states cross the Fermi edge, as can be seen by a comparison with the reference spectra collected from the gold film deposited on the sample holder.

In addition to the lower intensity, the Ti^{3+} band of the 3-u.c. sample also displays a smaller width at half maximum (0.9 eV) with respect to the 5-u.c. case (1.0 eV). This effect has also been observed in core-level photoemission spectra of the Ti $2p$ and Sr $3d$ core lines collected on the same samples [20] and tentatively ascribed to different band-bending effects.

It is rather interesting to observe that interface states are different from those expected for a conducting (Nb-doped) $SrTiO_3$ layer (Fig. 3, right panel, adapted from Ref. [38]), as the spectral weight is spread in a narrower energy region and there is no clear distinction between the incoherent emission (defect states at high BE) and the coherent emission at E_F. This indicates that the states observed at E_F in the LAO-STO interface are distinctive of the heterojunction rather than being related to the surface of an isolated STO substrate. A difference also appears with respect to the data presented by Berner *et al.* (Fig. 3, right panel, adapted from Ref. [19]) on conducting 5-u.c. LAO-STO samples measured at 20 K, where two distinct emissions at E_F (B) and about 1.5 eV below E_F (A) were observed, the former being the coherent emission with E_F crossing at the Γ point, while the latter was ascribed to Ti^{3+} states. Furthermore, if we consider the TiO_2 termination of the STO substrate and assume a TiO_2 single crystal as a reference system for the STO termination, it is known that defects in this layer may contribute to in-gap states far from E_F even in slightly substoichiometric rutile samples (Fig. 3, right panel [39]), at an energy distinctively different from the $3d^1$ states probed in the present experiment.

Also, oxygen vacancies can provide excess charge that eventually fills the STO states at the interface [40]. The present samples have been grown in an oxygen-rich atmosphere ($P_{O_2} \sim 10^{-3}$ mbar), which places them quite far from the conditions ($P_{O_2} \sim 10^{-6}$ mbar) where a relevant effect of the oxygen vacancies is expected [7]. Therefore, for the present samples oxygen vacancies are not expected to be the major source of doping.

Finally, it is worth observing that a model compound for the LAO-STO interface can also be the $La_xSr_{1-x}TiO_3$ system, as interdiffusion of La into the STO lattice observed in LAO-STO (see, e.g., Refs. [24–26]) may lead to the formation of mixed La-Sr-Ti oxide phases. For the $La_xSr_{1-x}TiO_3$ system, both an emission at E_F and a broad band peaked at about BE = 1.5 eV are observed (Fig. 3, right panel, adapted from Ref. [41]), the latter also being present in undoped $LaTiO_3$ single crystals [42]. The common understanding is that La substitution introduces electrons into the conduction band of $SrTiO_3$, a spectral weight at E_f appears, and $La_xSr_{1-x}TiO_3$ becomes metallic for x as small as 0.1 [41]. In this case, cation substitution would act as a doping mechanism, similar to what happens in, e.g., La-Sr-Cu-O superconducting cuprates. However, no similarity is found between our sample and the case of $La_xSr_{1-x}TiO_3$, suggesting that the observed states cannot be related to interdiffusion in a straightforward way. In fact, we observe states at E_F as if charges are injected into $SrTiO_3$ by Sr substitution with La, but we do not observe the band peaked at BE = 1.5 eV, characteristic also of undoped $LaTiO_3$ [42].

The ResPES chemical selectivity has also been exploited by collecting photoemission data also at the La $M_{4,5}$ edge

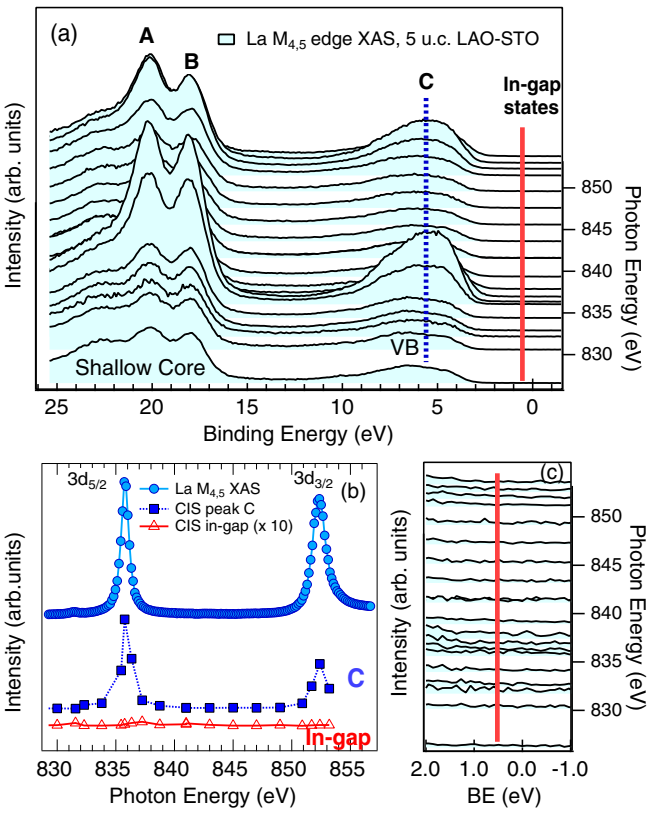

FIG. 4. (Color online) (a) ResPES data collected at the La $M_{4,5}$ edge, in the VB and shallow-core-levels region of the 5-u.c. sample. (b) XAS spectrum and CIS curves collected at the La $M_{4,5}$ on the 5-u.c. sample. The CIS curves have been tracked for the C band at BE = 5.5 eV (in panel A) and for the in-gap states at BE = 0.5 eV. (c) Enlarged view of the photoemission spectra in the 0.0–2.0 BE range.

[Fig. 4(a)]. Here, ResPES experiments carried out by scanning the photon energy at the La $M_{4,5}$ edge provides the opportunity to resonantly enhance the contribution of lanthanum-related electronic f states in the valence band, in the gap, and at E_F. The case of La is quite similar to that of Ti, and it can also be formally treated within a CI calculation scheme which includes CT configurations. CT effects are well known in core-level spectroscopy of ionic La compounds [43,44], and are likewise expected in the final state of the valence-band photoemission. In the La case, the ground state (g.s.) of a La^{3+} ion can be treated as

$$\Psi_{\text{g.s.}} = \alpha_0|4f^0\rangle + \alpha_1|4f^1\underline{L}^1\rangle + \alpha_2|4f^2\underline{L}^2\rangle, \quad (7)$$

while the final state of the XAS process (i.e., the intermediate state of the autoionization channel, i.s.) is

$$\Psi_{\text{i.s.}} = \beta_0|\underline{3d}4f^1\rangle + \beta_1|\underline{3d}4f^2\underline{L}^1\rangle + \beta_2|\underline{3d}4f^3\underline{L}^2\rangle, \quad (8)$$

and finally the photoemission channel (finale state, f.s.) is

$$\Psi_{\text{f.s.}} = \gamma_0|4f^0\underline{L}^1\rangle + \gamma_1|4f^1\underline{L}^2\rangle. \quad (9)$$

The results are shown in Fig. 4(a). In a simple single-configuration atomic view, the XAS transition at the La $M_{4,5}$ edge drives the system from the $3d^{10}4f^0$ initial state to the $3d^9 4f^1$ final state that is split into two peaks ($3d_{5/2}$ and $3d_{3/2}$) by the dominant spin-orbit interaction of the $3d$ electrons [Fig. 4(b)]. The CIS profile for states around BE $= 5.5 \pm 1.0$ eV [Fig. 4(b)] shows a resonant enhancement through the La edge, as expected from La-related states contributing to the valence band. On the contrary, the CIS profile for states at BE $= 0.5 \pm 1.0$ eV does not show any resonant enhancement. Here ± 1.0 eV represents the width of the region, centered either at BE $= 5.5$ eV or at BE $= 0.5$ eV, considered to extract the CIS profile. As shown in Fig. 4(c), the spectral weight in the 0.0–2.0 eV BE range is virtually flat and intensity variations are comparable to the noise level. In the event of $LaTiO_3$ segregations due to interdiffusion at the interface, the lack of La-related spectral weight at E_F is expected. In fact, La $4f$ states are predicted to be nearly 4 eV above the conduction-band minimum (see, e.g., Fig. 7(a) in Ref. [45]). This virtually leaves the spectral weight at E_F to Ti-derived states of STO.

Consistently, the RSW of Fig. 3 (left panel) represents the Ti $3d$ spectral weight in the VB region, as well as in the gap of $SrTiO_3$. In fact, most of the features of the VB occupied states can be described with DFT calculations of bulk $SrTiO_3$. However, the minimum energy separation (about 2.2 eV) between the Ti^{3+} states and the top of the valence band is smaller than the value of the bulk STO band gap (3.2 eV). Therefore the in-gap states should not be related to a simple filling of bulklike Ti $3d$ empty states of STO, but to a filling of Ti $3d^1$ states, pinned below E_F by band bending at the interface. Furthermore, if the DOS of the whole HJ is considered, plane projected DOS calculations (see, e.g., Ref. [46]), also indicate that about 2 eV above the top of the valence band, STO-related states can be found to be filled by electrons originating from the topmost LAO layers.

As in the case of the $3d$ states in Ti $L_{2,3}$ ResPES, the RSW at the La $M_{4,5}$ edge can be fairly described with f-DOS DFT calculations (Fig. 5). Therefore the resonating contribution of $4f$ electronic levels, along with that of Ti $3d$, can be used to pinpoint the energy position of the LAO valence band edge with respect to the STO VB edge ($\Delta^{\text{int}}_{\text{VBM}} = -0.7$ eV, inset of Fig. 5), assuming the absence of band bending in the LAO overlayer, as shown by the lack of broadening of La core-level states observed by x-ray photoemission in the same samples [20]. This is also consistent with the lack of La-O spectral weight at E_F. In fact, the presence of a potential gradient in the LAO overlayer should push valence-band states towards the Fermi level, and a spectral weight should be observed at or near E_F due to the occupied electronic states in the LAO surface layer [22].

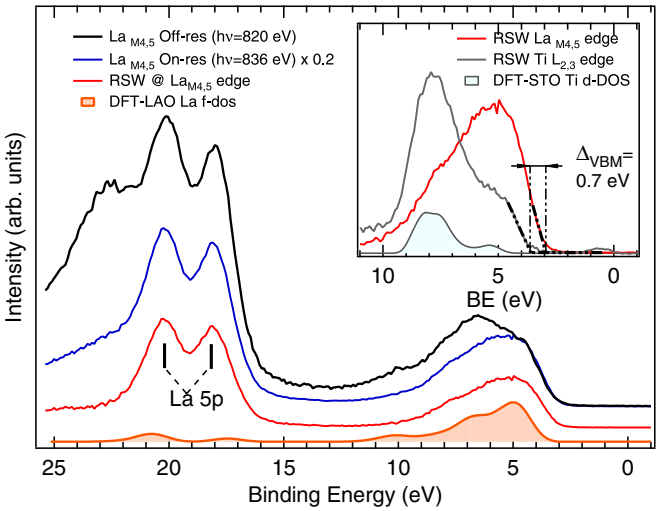

FIG. 5. (Color online) Photoemission spectra of 5-u.c. LAO-STO heterostructure at the La $M_{4,5}$ edge, collected out-of-resonance (black, $h\nu = 820$ eV) and on-resonance (blue, $h\nu = 836$ eV (scaled by a factor of 0.2) conditions. Spectral difference (red line) and f-DOS DFT calculations on a LAO bulk crystal (filled orange). (Inset) Comparison of La $4f$ and Ti $3d$ resonating contribution with d-DOS DFT calculations on a STO bulk crystal (filled gray).

B. Band alignment at the interface: Conducting vs insulating samples

The results discussed so far can be rationalized in the electronic band energy diagram shown in Fig. 6. A relevant bending of the conduction band is needed at the interface in order to account for the 2DEG spectroscopic signature.

The extent of the notch depends on several factors that need to be accounted for. If the width of the interface state contribution is regarded (inset of Fig. 3), the bending becomes 1.0 ± 0.1 eV. We consider this value as an *upper limit* for the bending, as the band diagram should be drawn by accounting for the experimental linewidth (0.40 eV, as can be extracted from the gold Fermi edge measured in the same conditions). This reduces the width of the IS peak to about 0.92 eV. Furthermore, we can regard the IS peak as a superposition of several peaks, each one shifted by the internal field found at a specific depth. For instance, if we consider an extent of 3 u.c. for the bending, on the basis of the calculations presented in the next section, the superposition of three peaks (FWHM $= 0.4$ eV each) distributed over a 0.6-eV energy range yields an overall width of 0.90 eV, in agreement with the

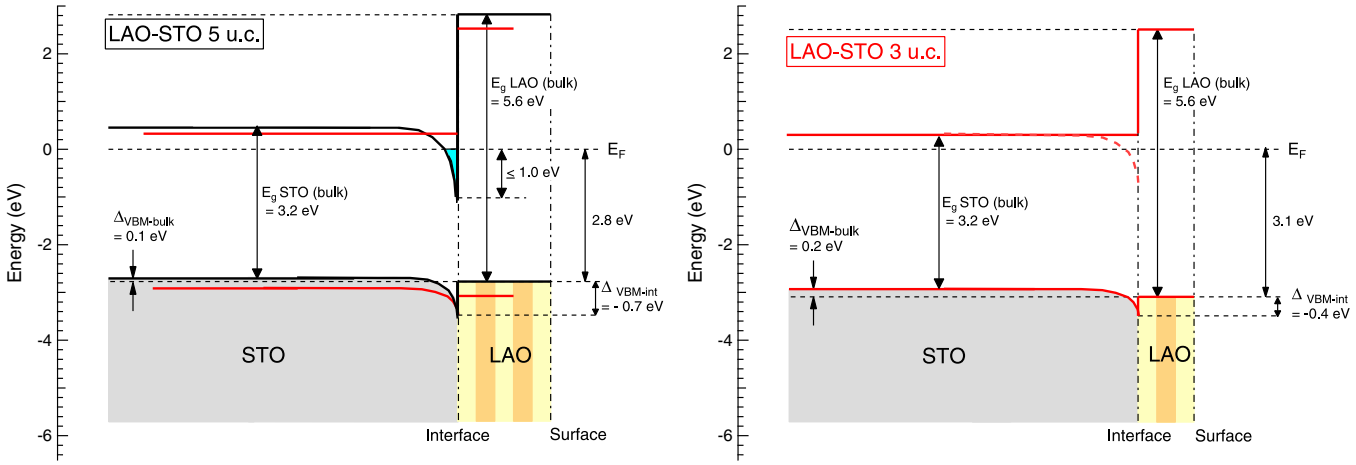

FIG. 6. (Color online) (Left) Band diagram for the LAO-STO 5-u.c. heterojunction. The horizontal red lines represent the energy shift for the 3-u.c. sample. (Right) Band diagram for the LAO-STO 3-u.c. heterojunction. All energies are defined within ±0.1 eV, with the exception of $\Delta^{\rm int}_{\rm VBM}$ values (±0.2 eV).

experimental finding of 0.92 eV. On this basis, we can estimate a depth of 0.6 eV for the notch. This agrees with the $\sigma_{\rm EXTRA}$ values extracted from the x-ray photoelectron spectroscopy (XPS) data (Table I of Ref. [20]). If $\sigma_{\rm EXTRA}$ is regarded as the contribution of the internal field to the overall linewidth, the value for Ti $2p$ (0.56 eV) agrees with the present estimate on Ti $3d$ levels (0.6 eV). The comparison with recent experimental findings and the underlying theoretical calculations is also helpful to discuss the present results. Cancellieri *et al.*[47] have found IS with a width of about 0.1 eV measured at $T = 11$ K in samples displaying $n_s = 6.5 \times 10^{13}$ cm^2, in agreement with calculations based on a charge transfer $Q = 0.1$ electrons/u.c. Even deeper bands (down to 0.4 eV below E_F at the Γ point) are expected [48] for charge densities of about 10^{14} cm^{-2}. This prediction is therefore consistent with our results on the 5-u.c. sample (0.6 eV) that features a measured charge density of 1.4×10^{14} cm^{-2}.

At the interface the valence-band shift is $\Delta^{\rm int}_{\rm VBM} = -0.7$ eV with respect to the LAO valence-band maximum (VBM). According to the fitting of shallow core-level and valence-band spectra presented in Ref. [20], below the interface the STO VBM is found above the LAO VBM, and $\Delta^{\rm bulk}_{\rm VBM} = 0.1 \pm 0.2$ eV. Therefore, assuming an energy gap of 3.2 eV for bulk STO, the conduction-band minimum (CBm) is found 0.5 ± 0.2 eV above E_F, yielding a remarkably notched energy-level profile. This value is higher with respect to the one (0.28 eV) measured by cross-sectional scanning tunneling microscopy [14], but in the light of experimental indeterminacy the two results can be regarded as consistent with each other. Furthermore, the CBm for the 3-u.c. sample is 0.3 eV above E_F, i.e., 0.2 eV lower than the case of the 5-u.c. sample (0.5 eV). This difference is comparable with the experimental error (±0.2 eV) for the estimate of the energy-level alignment in bulk STO.

Therefore, the results show that 5-u.c. conducting LAO-STO sample is a straddling gap (i.e., type I) heterojunction, in agreement with the experimental evidence provided in Refs. [14] and [23], but at odds with other studies on HJ alignment based on the analysis of XPS data [21,22]. In particular, the difference with respect to the results presented in Ref. [22] for a 5-u.c. sample grown at $P(O_2) = 1 \times 10^{-4}$ mbar are due to the different alignment of VBM of STO with respect to LAO ($\Delta^{\rm bulk}_{\rm VBM} = 0.3$ eV), resulting in a straddling gap (type II) HJ. In the 3-u.c. case, the VBM shifts to higher BE [$\rm VBM_{3uc}$ vs $\rm VBM_{5uc}$, Fig. 2(a)] and the $\Delta^{\rm int}_{\rm VB}$ value is reduced to −0.4 eV (Fig. 6, right panel). As $\Delta^{\rm bulk}_{\rm VB}$ was estimated to be 0.2 ±0.2 eV from XPS data [20], also in this case the HJ could be classified as type I (straddling gap). Finally, the CBm of STO is found 0.3 ± 0.2 eV above E_F. It is worth observing that when a relatively small value for $\Delta^{\rm bulk}_{\rm VB}$ is retrieved from the fitting of the valence-band photoemission data, the discrimination between a type-I and a type-II junction can be affected by some degree of uncertainty, here estimated as ±0.2 eV. As we regarded the IS observed in the 3-u.c. sample of extrinsic origin, the notch in the conduction-band profile is marked with a dashed line to underscore the difference with respect to the 5-u.c. case.

C. Estimation of the 2DEG layer thickness

Finally, taking as a reference the $\Delta^{\rm bulk}_{\rm VB} - \Delta^{\rm int}_{\rm VB}$ energy difference, a simulation has been developed with the aim to evaluate the extension of the 2DEG below the interface. The calculation was carried out by considering the photoemission intensity attenuation obtained through the depth distribution function (DDF). As shown in the following, such a $\Delta^{\rm bulk}_{\rm VB} - \Delta^{\rm int}_{\rm VB}$ energy offset is compatible with a scenario where the 2DEG is confined within the first three unit cells below the interface, in agreement with the estimate based on core-level data and transport properties [20]. The interface has been simulated as a sequence of 3.8-Å -thick STO single layers (u.c.), where the BE of the photoemission peak of each layer is energy shifted in order to mimic the notched energy-band profile [inset of Fig. 7(a)]. Changes of the unit-cell thickness in the 3.7–3.9 Å range to account for strain effects at the interface yield negligible energy shifts (less than 0.02 eV) that do not affect the results discussed so far.

In Fig. 7(a) the Ti $3d$ photoemission peak intensity for electrons coming from the uppermost STO layers has been calculated for different photon energies. As can be seen from

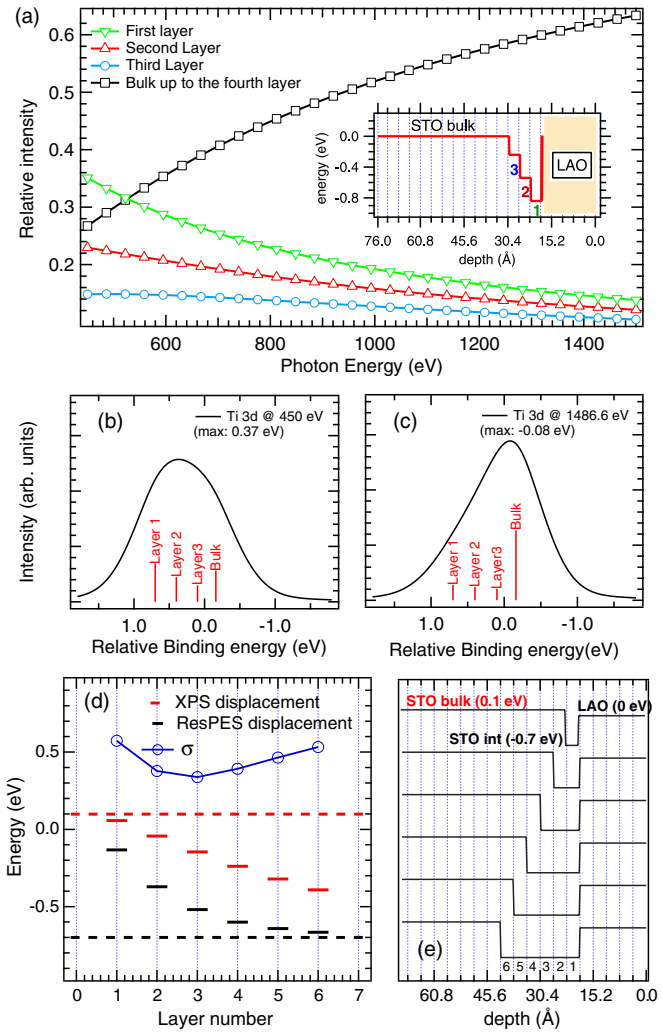

FIG. 7. (Color online) (a) DDF-based calculation of the contribution to Ti $3d$ photoemission peak intensity of the first three STO layers and of the bulk in the 450.0–1500 eV photon energy range. The band profile depicted in the inset has been considered for the calculation. This profile has been drawn on the basis of the energy profile shown in Fig. 6. (b, c) Calculated photoemission spectra for Ti $3d$ levels at $h\nu = 450.0$ and $h\nu = 1486.6$ eV. (d) Calculation of the XPS Ti $3p$ (black) and ResPES Ti $3d$ (red) photoemission peak shifts for the various band profiles shown in (e). The horizontal dashed lines represent the observed Δ_{VB}^{int} and Δ_{VB}^{bulk} values, while the blue line represents the standard deviation (σ).

Fig. 7(a), the first three STO layers contribute to nearly 72% of the spectral weight in the ResPES regime (photon energy at 450 eV) but only to 35% in the XPS regime ($h\nu = 1486.6$ eV).

Furthermore, as the photon energy is swept from 450 to 1500 eV, not only the weight of the single layers in the photoemission peak changes, but also the overall peak line shape and binding energy. For example, assuming as a model of a triangular notch the stepped band profile shown in the inset of Fig. 7(a), the photoemission peaks for the low (450 eV) and high (1486.6 eV) photon energy spectra have been calculated, as shown in Figs. 7(b) and 7(c). This calculation simulates a photoemission process from Ti $3d$ levels at the resonant threshold (b), as well as in an XPS-like experiment (c). The calculation has then been extended to several energy-level profiles. Figure 7(d) shows the average peak positions for the various model profiles of the HJ band levels represented in Fig. 7(e); the blue line shows the standard deviation σ with respect to the measured values (−0.7 eV for ResPES and +0.10 eV for XPS). As the extent of the notched region increases, the overall peak positions move towards the interface value (−0.7 eV), while a contraction of the band profile notch pushes both peak positions towards the bulk values (+0.1 eV). The best match with both reference values [dashed horizontal lines in Fig. 7(d)], marked by the minimum of σ (blue line), is found for a band-bending depth of about 2–3 unit cells.

IV. CONCLUSIONS

We have investigated, through element-specific spectroscopies, the origin of the interface states in a conducting LAO-STO heterointerface. We have shown that these states, found at E_F, can be ascribed to an intrinsic effect of the polar field, as cation mixing does not seem to affect the spectral weight of interface states, and the observed $3d^1$ interface states are different from those reported for conducting Nb:STO surfaces, defected TiO_2 surfaces, or $La_{1-x}Sr_xTiO_3$, that at different extents may be regarded as reference systems for the LAO-STO heterointerface. The same spectroscopic tools have also allowed us to track the band profile at the interface. The results show that both heterointerfaces are type I.

Differences between the two interfaces under consideration (i.e., a conducting 5-u.c. interface and and insulating 3-u.c. interface prepared under the same growth conditions) are represented by the larger notch in the valence-band energy profile observed in the conducting interface. Furthermore, the conducting sample displays a deep notch of intrinsic IS, whose width is estimated to be about 0.6 eV and, in any case, not larger than 1 eV.

Finally, it is shown that the $\Delta_{VB}^{bulk} - \Delta_{VB}^{int}$ energy offset for the 5-u.c. layer is compatible with a scenario where the 2DEG is confined within the first three unit cells below the interface, in agreement with the estimate based on core-level data and transport properties [20].

Differences with the band profiling so far proposed for similar systems can be ascribed to subtle changes in the growth conditions, disclosing a rich scenario of electronic properties driven by oxygen stoichiometry.

[1] A. Ohtomo, D. A. Muller, J. L. Grazul, and H. Y. Hwang, Nature (London) **419**, 378 (2002).

[2] A. Ohtomo and H. Y. Hwang, Nature (London) **427**, 423 (2004).

[3] H. Y. Hwang, Y. Iwasa, M. Kawasaki, B. Keimer, N. Nagaosa, and Y. Tokura, Nature Mater. **11**, 103 (2012).

[4] S. Thiel, G. Hammer, A. Schmehl, C. W. Schneider, and J. Mannhart, Science **313**, 1942 (2006).

[5] N. Reyren, S. Thiel, A. D. Caviglia, L. Fitting Kourkoutis, G. Hammerl, C. Richter, C. W. Schneider, T. Kopp, A. S. Retschi, D. Jaccard, M. Gabay, D. A. Muller, J. M. Triscone, and J. Mannhart, Science **317**, 1196 (2007).

[6] A. Brinkman, M. Huijben, M. van Zalk, J. Huijben, U. Zeitler, J. K. Maan, W. G. van der Wiel, G. Rijnders, D. H. A. Blank, and H. Hilgenkamp, Nature Mater. **6**, 493 (2007).

[7] M. Huijben, A. Brinkman, G. Koster, G. Rijnders, H. Hilgenkamp, and D. H. A. Blank, Adv. Mater. **21**, 1665 (2009).

[8] Z. Q. Liu, C. J. Li, W. M. Lü, X. H. Huang, Z. Huang, S. W. Zeng, X. P. Qiu, L. S. Huang, A. Annadi, J. S. Chen, J. M. D. Coey, T. Venkatesan, and Ariando, Phys. Rev. X **3**, 021010 (2013).

[9] E. Assmann, P. Blaha, R. Laskowski, K. Held, S. Okamoto, and G. Sangiovanni, Phys. Rev. Lett. **110**, 078701 (2013).

[10] H. Liang, L. Cheng, X. Zhai, N. Pan, H. Guo, J. Zhao, H. Zhang, L. Li, X. Zhang, X. Wang, C. Zeng, Z. Zhang, and J. G. Hou, Sci. Rep. **3**, 1975 (2013).

[11] S. Wu, X. Luo, S. Turner, H. Peng, W. Lin, J. Ding, A. David, B. Wang, G. Van Tendeloo, J. Wang, and T. Wu, Phys. Rev. X **3**, 041027 (2013).

[12] C. W. Bark, P. Sharma, Y. Wang, S. H. Baek, S. Lee, S. Ryu, C. M. Folkman, T. R. Paudel, A. Kumar, S. V. Kalinin, A. Sokolov, E. Y. Tsymbal, M. S. Rzchowski, A. Gruverman, and C. B. Eom, Nano Lett. **12**, 1765 (2012).

[13] A. Kumar, T. M. Arruda, Y. Kim, I. N. Ivanov, S. Jesse, C. W. Bark, N. C. Bristowe, E. Artacho, P. B. Littlewood, C.-B. Eom, and S. V. Kalinin, ACS Nano **6**, 3841 (2012).

[14] B.-C. Huang, Y.-P. Chiu, P.-C. Huang, W.-C. Wang, V. T. Tra, J.-C. Yang, Q. He, J.-Y. Lin, C.-S. Chang, and Y.-H. Chu, Phys. Rev. Lett. **109**, 246807 (2012).

[15] W. Siemons, G. Koster, H. Yamamoto, T. H. Geballe, D. H. A. Blank, and M. R. Beasley, Phys. Rev. B **76**, 155111 (2007).

[16] G. Drera, F. Banfi, F. Federici Canova, P. Borghetti, L. Sangaletti, F. Bondino, E. Magnano, J. Huijben, M. Huijben, G. Rijnders, D. H. A. Blank, H. Hilgenkamp, and A. Brinkman, Appl. Phys. Lett. **98**, 052907 (2011).

[17] A. Koitzsch, J. Ocker, M. Knupfer, M. C. Dekker, K. Dörr, B. Buchner, and P. Hoffmann, Phys. Rev. B **84**, 245121 (2011).

[18] C. Cancellieri, M. L. Reinle-Schmitt, M. Kobayashi, V. N. Strocov, T. Schmitt, P. R. Willmott, S. Gariglio, and J.-M. Triscone, Phys. Rev. Lett. **110**, 137601 (2013).

[19] G. Berner, M. Sing, H. Fujiwara, A. Yasui, Y. Saitoh, A. Yamasaki, Y. Nishitani, A. Sekiyama, N. Pavlenko, T. Kopp, C. Richter, J. Mannhart, S. Suga, and R. Claessen, Phys. Rev. Lett. **110**, 247601 (2013).

[20] G. Drera, G. Salvinelli, A. Brinkman, M. Huijben, G. Koster, H. Hilgenkamp, G. Rijnders, D. Visentin, and L. Sangaletti, Phys. Rev. B **87**, 075435 (2013).

[21] L. Qiao, T. C. Droubay, T. C. Kaspar, and S. A. Chambers, Surf. Sci. **605**, 1381 (2011).

[22] G. Berner, A. Müller, F. Pfaff, J. Walde, C. Richter, J. Mannhart, S. Thiess, A. Gloskovskii, W. Drube, M. Sing, and R. Claessen, Phys. Rev. B **88**, 115111 (2013).

[23] Y. Segal, J. H. Ngai, J. W. Reiner, F. J. Walker, and C. H. Ahn, Phys. Rev. B **80**, 241107 (2009).

[24] S. A. Chambers, M. H. Englehard, V. Shutthanandan, Z. Zhu, T. C. Droubay, T. Feng, H. D. Lee, T. Gustafsson, E. Garfunkel, A. Shah, J. M. Zuo, and Q. M. Ramasse, Surf. Sci. Rep. **65**, 317 (2010).

[25] V. Vonk, J. Huijben, D. Kukuruznyak, A. Stierle, H. Hilgenkamp, A. Brinkman, and S. Harkema, Phys. Rev. B **85**, 045401 (2012).

[26] P. R. Willmott, S. A. Pauli, R. Herger, C. M. Schleputz, D. Martoccia, B. D. Patterson, B. Delley, R. Clarke, D. Kumah, C. Cionca, and Y. Yacoby, Phys. Rev. Lett. **99**, 155502 (2007).

[27] X. Gonze, B. Amadon, P.-M. Anglade, J.-M. Beuken, F. Bottin, P. Boulanger, F. Bruneval, D. Caliste, R. Caracas, M. Cote, T. Deutsch, L. Genovese, Ph. Ghosez, M. Giantomassi, S. Goedecker, D. R. Hamann, P. Hermet, F. Jollet, G. Jomard, S. Leroux, M. Mancini, S. Mazevet, M. J. T. Oliveira, G. Onida, Y. Pouillon, T. Rangel, G.-M. Rignanese, D. Sangalli, R. Shaltaf, M. Torrent, M. J. Verstraete, G. Zerah, and J. W. Zwanziger, Comp. Phys. Commun. **180**, 2582 (2009).

[28] J. J. Yeh and I. Lindau, At. Data Nucl. Data Tables **32**, 1 (1985).

[29] W. S. M. Werner, Surf. Interface Anal. **31**, 141 (2001).

[30] S. Tanuma, C. J. Powell, and D. R. Penn, Surf. Interface Anal. **21**, 165 (1994).

[31] G. Drera, G. Salvinelli, J. Åhlund, P. G. Karlsson, B. Wannberg, E. Magnano, S. Nappini, and L. Sangaletti, J. Electron Spectrosc. Relat. Phenom. **195**, 109 (2014).

[32] S. Hüfner, S.-H. Yang, B. S. Mun, J. Schaefer, E. Rotenberg, C. S. Fadley, and S. D. Kevan, Phys. Rev. B **61**, 12582 (2000).

[33] K. Okada and A. Kotani, J. Electron Spectrosc. Relat. Phenom. **62**, 131 (1993).

[34] M. Salluzzo, J. C. Cezar, N. B. Brookes, V. Bisogni, G. M. De Luca, C. Richter, S. Thiel, J. Mannhart, M. Huijben, A. Brinkman, G. Rijnders, and G. Ghiringhelli, Phys. Rev. Lett. **102**, 166804 (2009).

[35] U. Fano, Phys. Rev. **124**, 1866 (1961).

[36] L. H. Tjeng, C. T. Chen, J. Ghijsen, P. Rudolf, and F. Sette, Phys. Rev. Lett. **67**, 501 (1991).

[37] S. Pagliara, L. Sangaletti, A. Goldoni, C. Kim, Z.-X. Shen, A. Revcolevschi, G. Dhalenne, and F. Parmigiani, Phys. Rev. B **65**, 205107 (2002).

[38] Y. Ishida, R. Eguchi, M. Matsunami, K. Horiba, M. Taguchi, A. Chainani, Y. Senba, H. Ohashi, H. Ohta, and S. Shin, Phys. Rev. Lett. **100**, 056401 (2008).

[39] G. Drera, L. Sangaletti, F. Bondino, M. Malvestuto, L. Malavasi, Y. Diaz-Fernandez, S. Dash, M. C. Mozzati and P. Galinetto, J. Phys.: Condens. Matter **25**, 075502 (2013).

[40] C. Cancellieri, N. Reyren, S. Gariglio, A. D. Caviglia, A. Fete, and J.-M. Triscone, Europhys. Lett. **91**, 17004 (2010).

[41] A. Fujimori, I. Hase, M. Nakamura, H. Namatame, Y. Fujishima, Y. Tokura, M. Abbate, F. M. F. de Groot, M. T. Czyzyk, J. C. Fuggle, O. Strebel, F. Lopez, M. Domke, and G. Kaindl, Phys. Rev. B **46**, 9841(R) (1992).

[42] M. W. Haverkort, Z. Hu, A. Tanaka, G. Ghiringhelli, H. Roth, M. Cwik, T. Lorenz, C. Schüßler-Langeheine, S. V. Streltsov, A. S. Mylnikova, V. I. Anisimov, C. de Nadai, N. B. Brookes, H. H. Hsieh, H.-J. Lin, C. T. Chen, T. Mizokawa, Y. Taguchi,

Y. Tokura, D. I. Khomskii, and L. H. Tjeng, Phys. Rev. Lett. **94**, 056401 (2005).

[43] M. F. Sunding, K. Hadidi, S. Diplas, O. M. Lovvik, T. E. Norby, and A. E. Gunnæs, J. Electron Spectrosc. Relat. Phenom. **184**, 399 (2011).

[44] C. Dallera, K. Giarda, G. Ghiringhelli, A. Tagliaferri, L. Braicovich, and N. B. Brookes, Phys. Rev. B **64**, 153104 (2001).

[45] F. Iori, M. Gatti, and A. Rubio, Phys. Rev. B **85**, 115129 (2012).

[46] Y. Li, S. Na Phattalung, S. Limpijummong, J. Kim, and J. Yu, Phys. Rev. B **84**, 245307 (2011).

[47] C. Cancellieri, M. L. Reinle-Schmitt, M. Kobayashi, V. N. Strocov, P. R. Willmott, D. Fontaine, Ph. Ghosez, A. Filippetti, P. Delugas, and V. Fiorentini, Phys. Rev. B **89**, 121412(R) (2014).

[48] P. Delugas, A. Filippetti, V. Fiorentini, D. I. Bilc, D. Fontaine, and P. Ghosez, Phys. Rev. Lett. **106**, 166807 (2011).